Cooperativity between the Silver(I) and Iodine(III) Centers in Electrophilic Activation of Organic Substrates

Mikhail V. Il'in,[1] Denis A. Polonnikov,[1] Alexander S. Novikov,[1,2] Alexandra A. Sysoeva,[1] Yana V. Safinskaya,[1] Sevilya N. Yunusova,[1] and Dmitrii S. Bolotin*[1]

[1] Institute of Chemistry, Saint Petersburg State University, Universitetskaya Nab. 7/9, Saint Petersburg, 199034, Russian Federation

[2] Research Institute of Chemistry, Peoples' Friendship University of Russia (RUDN University), Miklukho-Maklaya St. 6, Moscow, 117198, Russian Federation

* Corresponding author E-mail: d.s.bolotin@spbu.ru

Kinetic data and computational study indicate that in the solution, pyrazole-containing iodolium salts and silver(I) center bind each other, and such interplay significantly affect the total catalytic activity of mixture of these Lewis acids compared with separate catalysis of the reactions required electrophilic activation of carbonyl, imino group, or triple CC bond. Moreover, the kinetic data and ^{1}H NMR monitoring indicate that such cooperation results in prevention of decomposition of the organocatalysts by the silver(I) center during the reaction progress. XRD study indicates that in the solid state, the iodolium triflates and silver(I) triflate associate each other to give the complex species featuring triflate-bridged iodine(III) and silver(I) centers: a rare example of square-planar silver(I) complex and pentacoordinated trigonal bipyramidal dinuclear silver(I) complex.

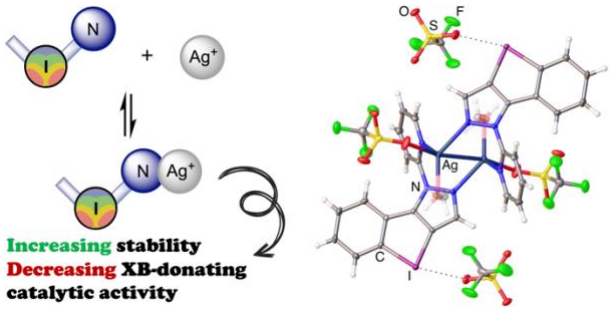

Introduction

Recently, significant research efforts have been focused on exploring new types of organocatalysts due to their significant advantages over organometallic and metal-complex catalysts, including low to negligible sensitivity to air and moisture, less environmental impact, and lower toxicity.[1, 2] In general, organocatalysts can bind to a substrate either via covalent or non-covalent interactions to promote a chemical reaction. The former activation mode involves the formation of one or several covalent bonds between the catalyst and a reaction substrate. Typically, amines,[1-5] phosphines,[6] or heterocyclic carbenes[1, 7, 8] comprise this type of organocatalyst. The latter mode of activation involves non-covalent interactions between the catalyst and the substrate, and such type organocatalyst interacting with a substrate via noncovalent interactions (for example, ureas,[9-14] squaramides,[14-16] and other Brønsted acids,[17-19]) typically does so through hydrogen bonding (HB). Nevertheless, σ-hole donating species binding to reaction substrates via chalcogen (ChB) or halogen (XB) bonds—bonding between electron-deficient area on the surface of chalcogen or halogen atom and a Lewis base, respectively[20, 21]—provide a more directional orientation and a higher electrophilic activation of ligated species compared to well-studied HB donating organocatalysts. One of the most promising types of these organocatalysts are based on iodonium salts, which effectively catalyze a wide range of organic reactions.[22-32]

Despite the advantages of organocatalysts, metal-complex catalysis is still widely used in organic chemistry. Analysis of the current literature data indicates that although today there is a pronounced trend towards the use of metal-complex catalysts based on environmentally friendly and/or biocompatible metal centers, the use of noble group metal centers still occupies a leading position in some areas of application, in particular, selective *ortho*-[33, 34] and *meta*-functionalization[33, 35-41] of aromatic compounds and cross-coupling reactions, as well as hydrogenation[42, 43] and hydrosilylation[44, 45] processes.

Actual and growing trend in homogeneous catalysis is based on cooperative catalysis combining the advantages of both organic and transition metal catalysis under one-pot reaction conditions.[2, 46-48] Although the cooperative catalysis has been extensively studied for many common types of organocatalysts, application of XB-donating species in this field is still almost unexplored. Thus, tetratopic noncharged iodine(I)-based XB-donors were utilized as a template for ruthenium(II)-catalyzed macrocyclization of olefines,[49] whereas cationic iodine(I)- and iodine(III)-based XB-donors were utilized as a chloride-abstracting agents for in situ activation of gold(I)-containing catalysts.[25, 50, 51] These two examples represent an application of XB donors in the systems involving noble metal catalysis but none of them utilize the XB donor for the electrophilic activation of a reaction substrate.

Considering scarce data on simultaneous application of the XB donors and the noble metal centers in organic synthesis, further study of cooperative effects between these two types of Lewis acids requires additional study. In this work, we experimentally and theoretically studied the interplay between the external silver(I) center and iodine(III) center in a series of iodolium salts, which includes their complexation and cooperative catalysis of some organic transformations requiring electrophilic activation of carbonyl, imino group, or triple CC bond.

Results and Discussion

Selection of the XB-donating and noble metal-based Lewis acids. Current study of diaryliodonium-based noncovalent organocatalysts includes functionalization of the phenylene system in the iodine-containing cation[24, 52, 53] and preparation of the iodoniums featuring heteroaromatic moieties.[25] Dinuclear iodine(III)-containing species were also involved in the catalysis.[22, 26] Recently pyrazolyl-containing iodolium salts were shown to exhibit higher catalytic activity than the dibenziodolium analogue in the reaction of solvolysis of benzhydryl halides,[31] but it further was shown by us that the higher catalytic effect might be caused by partial decomposition of the catalyst, at least in the complex multicomponent reaction.[54] For this study, three pyrazolyl-containing iodonium triflates were chosen as model organocatalytic species, because they feature potentially nucleophilic N atom capable to bind to a metal-based Lewis acid (**Figure 1**). Dibenziodolium triflate has been chosen as a referent compound, which do not possess any heteroatoms, which can provide coordination to a metal center (**Figure 1**).

Previous works of other authors,[25, 50, 51] as well as our observations indicate that utilization of a noble metal halides or their other halogen-containing species results in abstraction of the halide ligand by the iodolium cation, which suppresses the electrophilicity of the latter and typically results in precipitation of the organic residues almost insoluble in many organic solvents. Thus, it was found by us that **Cat4**^{OTf} reacts with $K_2[PtCl_4]$ in H_2O to give insoluble in H_2O, EtOH, Me_2CO, and $CHCl_3$ platinum-containing residue and **Cat4**^{Cl} (which also almost insoluble in these solvents). A reaction of **Cat4**^{OTf} with $PdCl_2$ in MeOH resulted in precipitation of **Cat4**^{Cl} accompanied with formation of a series of unidentified palladium-containing species. Instantaneous precipitation of **Cat4**^{Cl} was also observed after mixing of MeOH solutions of **Cat4**^{OTf} and $NiCl_2$, $CoCl_2$, $CuCl_2$, or $ZnCl_2$. Considering this, AgOTf has been chosen as a model noble metal-containing compound, since availability of the triflate-anion excludes anion metathesis upon addition of any of **Cat1**^{OTf}–**Cat4**^{OTf} and this compound is relatively stable under mild conditions in the presence of oxygen and traces of water, as well as it has many applications in catalysis.[55-58]

Iodolium salt–silver(I) interplay in the solid state. To study possible binding modes between the iodolium salts **Cat1**^{OTf}–**Cat4**^{OTf} and AgOTf, cocrystals of these species were tried to obtain from MeOH solution. Mixtures of any of **Cat1**^{OTf}–**Cat4**^{OTf} and AgOTf (1:1 molar ratio) in MeOH were left to slow evaporation of the solvent under ambient conditions (ca. 20 °C in air). The crystals of **Cat1**$_3$[Ag(OTf)$_4$] suitable for single-crystal XRD study were obtained from the **Cat1**^{OTf}–AgOTf mixture (**Figure 2**). Many attempts to obtain crystals suitable for the XRD study from **Cat2**^{OTf}–AgOTf and **Cat3**^{OTf}–AgOTf mixtures were unsuccessful, whereas the crystals of [Ag$_2$(**Cat4**)$_2$(MeOH)$_2$(OTf)$_2$](OTf)$_2$ were obtained from the solution containing **Cat4**^{OTf}–AgOTf mixture (**Figure 3**). All attempts to obtain the complexes of other composition by preparation of the mixtures with other ratios of the reagents (**Cat**^{OTf}:AgOTf ranged from 4:1 to 1:4) led to the formation of the crystals of same complexes **Cat1**$_3$[Ag(OTf)$_4$] (for **Cat1**^{OTf}) and [Ag$_2$(**Cat4**)$_2$(MeOH)$_2$(OTf)$_2$](OTf)$_2$ (for **Cat4**^{OTf}) or formation of the unidentified solid mixtures containing the iodolium salt and AgOTf (for **Cat2**^{OTf} and **Cat3**^{OTf}).

The complex **Cat1**$_3$[Ag(OTf)$_4$] represents a rare example of square-planar silver(I) complex,[59] as well as consists of previously unknown triple-charged anion of silver(I) tetratriflate. This type of geometry might be stabilized via XBs between each triflate ligand and the

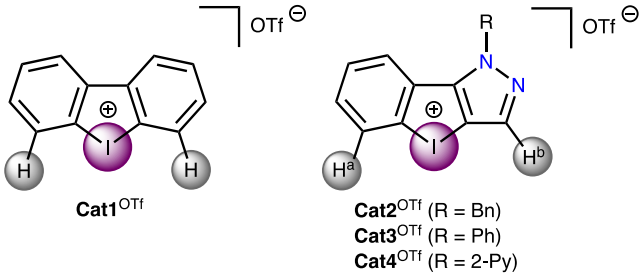

Cat1^{OTf} **Cat2**^{OTf} (R = Bn) **Cat3**^{OTf} (R = Ph) **Cat4**^{OTf} (R = 2-Py)

Figure 1. Iodonium salts **Cat1**^{OTf}–**Cat4**^{OTf} chosen as a model XB donors.

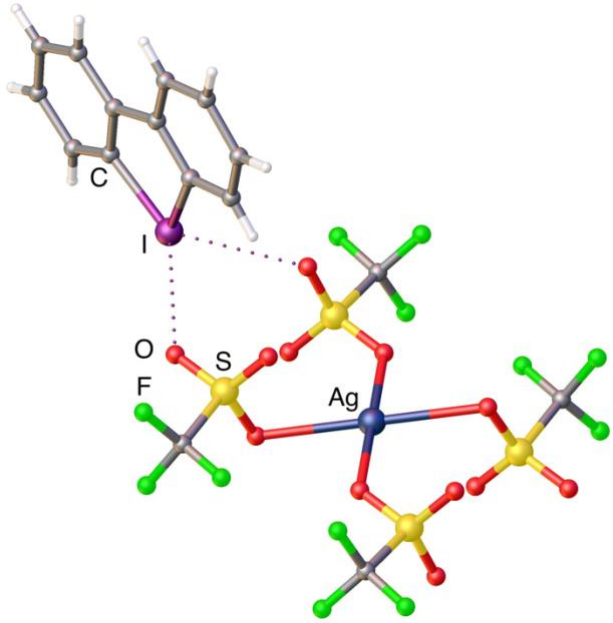

Figure 2. The molecular structure of **Cat1**$_3$[Ag(OTf)$_4$] exhibiting square-planar surrounding of the silver(I) center. Two dibenziodolium cations are omitted for clarity. Thermal ellipsoids are given at the 50% probability level.

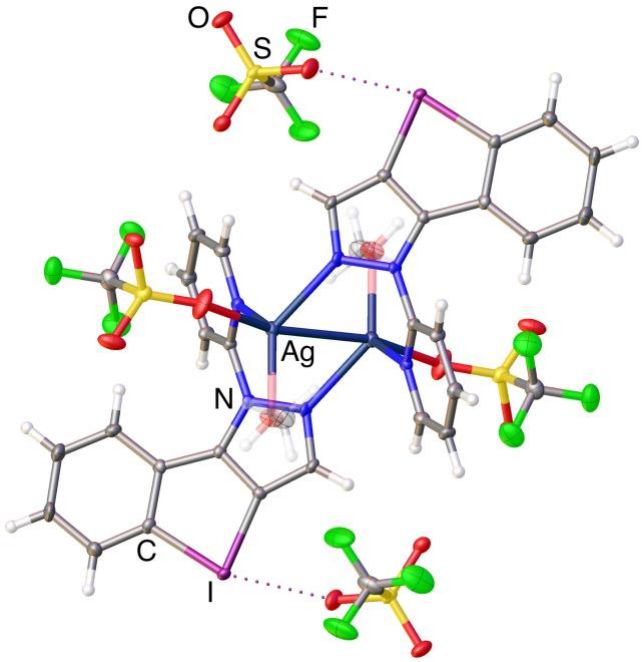

Figure 3. The molecular structure of [Ag$_2$(**Cat4**)$_2$(MeOH)$_2$(OTf)$_2$](OTf)$_2$ exhibiting trigonal bipyramidal surrounding of the silver(I) center. Thermal ellipsoids are given at the 50% probability level.

σ-holes of the **Cat1**$^{+}$ species. To verify this suggestion, the DFT calculations followed by the topological analysis of the electron density distribution within the QTAIM approach[60] were carried out at the ωB97XD/Sapporo-DZP level of theory for model supramolecular associate (see Computational details and Supporting Information). Results of QTAIM analysis are summarized in **Table 1**.

The QTAIM analysis of **Cat1**$_3$[Ag(OTf)$_4$] demonstrates the presence of bond critical points for intermolecular interactions I···O (**Table 1**). The low magnitude of the electron density (0.007–0.025 a.u.), positive values of the Laplacian of electron density (0.023–0.067 a.u.), and zero or very close to zero energy density in these bond critical points and estimated strength for appropriate short contacts (7.1–28.5 kJ mol^{-1}) are typical for noncovalent interactions. The balance between the Lagrangian kinetic energy G(**r**) and potential energy density V(**r**) at the bond critical points reveals the nature of these interactions, if the ratio –G(**r**)/V(**r**) > 1 is satisfied, the nature of appropriate interaction is purely non-covalent, in case the –G(**r**)/V(**r**) < 1 some covalent component takes place;[63] based on this criterion one can state that a covalent contribution in intermolecular interactions I···O in **Cat1**$_3$[Ag(OTf)$_4$] is absent (**Table 1**). The Laplacian of electron density is typically decomposed into the sum of contributions along the three principal axes of maximal variation, giving the three eigenvalues of the Hessian matrix (λ_1, λ_2 and λ_3), and the sign of λ_2 can be utilized to distinguish bonding (attractive, $\lambda_2 < 0$) weak interactions from non-bonding ones (repulsive, $\lambda_2 > 0$),[64, 65] and it indicates that discussed intermolecular interactions I···O are attractive (**Table 1**).

Additionally, we carried out geometry optimization procedure for square-planar and tetrahedral isomers of the anion [Ag(OTf)$_4$]$^{3-}$ in the gas phase (**Figure 4**) and found that the tetrahedral isomer is more stable than the square-planar isomer by 34.7 kJ mol^{-1}. Considering comparable energies of the XB in the crystal and difference in energy between two geometries at the silver(I) center, it is possible to expect that energetically unfavorable square-planar geometry of [Ag(OTf)$_4$]$^{3-}$ in the crystal is stabilized by the XBs.

The crystal structure of [Ag$_2$(**Cat4**)$_2$(MeOH)$_2$(OTf)$_2$](OTf)$_2$ also represents a rare example of pentacoordinated trigonal bipyramidal geometry of the silver(I) center.[66, 67] Similarly with the complex **Cat1**$_3$[Ag(OTf)$_4$], it includes the triflate ligands bridging the silver(I) and iodine(III) centers (not shown on **Figure 3** for simplicity). In addition, silver(I) centers bind N atoms in the pyrazole and pyridine rings.

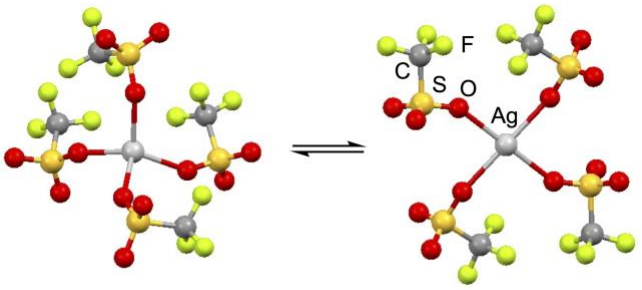

Tetrahedral geometry (0.0 kJ mol^{-1}) Square-planar geometry (34.7 kJ mol^{-1})

Figure 4. Calculated geometries and relative energy of [Ag(OTf)$_4$]$^{3-}$ isomers in the gas phase.

All these observations indicate that (i) cationic heterocyclic iodolium salts can be effectively utilized as ligands for functionalization of metal-based Lewis acids, at least in the solid state, (ii) bridging of the silver(I) and iodine(III) centers by the triflate is typical for the chosen system and is realized either for the dibenziodolium cation, which does not feature any nucleophilic heteroatoms, and pyrazolyl-containing iodolium cation **Cat4**$^{+}$. Considering these data, one can expect the cooperation of silver(I) and iodolium triflates in the solution.

Iodolium triflate–silver triflate interplay in the solution. To study binding of **Cat1**^{OTf}–**Cat4**^{OTf} with AgOTf, ^{1}H NMR titration of the catalysts by silver(I) triflate has been performed. Addition of the metal salt to the solutions of any of the catalysts in MeOH resulted in gradual shift in the positions of the resonance peaks attributed to the cations (**Figure 5**, left).

The K^{298} values calculated using Bindfit software using a 1:1 host–guest binding model were found to be equal 7.2±3.5 (for **Cat1**^{OTf}), 7.4±0.9 (for **Cat2**^{OTf}), 4.3±1.5 (for **Cat3**^{OTf}), 7.9±1.1 (for **Cat4**^{OTf}). The obtained values of K^{298} were further used for calculation of the Gibbs free energy of binding (**Figure 5**, right), whose mean values equal –4.9 kJ mol^{-1} (for **Cat1**^{OTf}), –5.0 kJ mol^{-1} (for **Cat2**^{OTf}), –3.6 kJ mol^{-1} (for **Cat3**^{OTf}), –5.1 kJ mol^{-1} (for **Cat4**^{OTf}). High relative value of standard deviation for the titration of **Cat1**^{OTf} by AgOTf can be explained in terms of significantly smaller changes in the chemical shift during the titration compared with that for **Cat2**^{OTf}–**Cat4**^{OTf}.

Table 1. Values of the density of all electrons – ρ(**r**), Laplacian of electron density – $\nabla^2\rho(\mathbf{r})$ and appropriate λ_2 eigenvalues, energy density – H_b, potential energy density – V(**r**), and Lagrangian kinetic energy – G(**r**) (a.u.) at the bond critical points (3, –1), corresponding to intermolecular interactions I···O in **Cat1**$_3$[Ag(OTf)$_4$], and estimated strength for these interactions E_{int} (kJ mol^{-1}).

Length of short I···O contacts*	ρ(**r**)	$\nabla^2\rho(\mathbf{r})$	λ_2	H_b	V(**r**)	G(**r**)	E_{int}[a]	E_{int}[b]
2.789 Å	0.025	0.066	–0.025	0.000	–0.016	0.016	28.5	28.0
2.819 Å	0.022	0.067	–0.022	0.001	–0.015	0.016	26.8	28.0
3.041 Å	0.016	0.046	–0.016	0.001	–0.010	0.011	18.0	19.2
3.261 Å	0.010	0.031	–0.010	0.001	–0.006	0.007	10.9	12.1
3.522 Å	0.007	0.023	–0.007	0.001	–0.004	0.005	7.1	8.9

* The Bondi's (shortest) van der Waals radii for iodine and oxygen atoms are 1.98 Å and 1.52 Å, respectively.[61] [a] $E_{int} = 0.68(-V(\mathbf{r}))$.[62] [b] $E_{int} = 0.67G(\mathbf{r})$.[62]

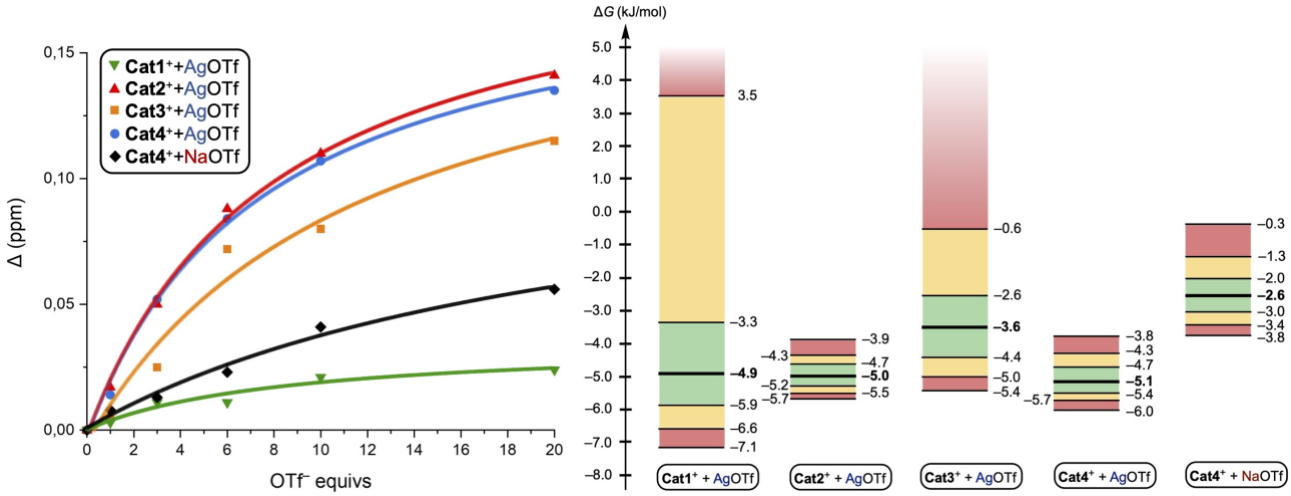

Figure 5. ^{1}H NMR titration at 298 K of any of **Cat1**^{OTf}–**Cat4**^{OTf} using AgOTf or NaOTf. The plot represents the shift of the resonance peak of *ortho*-Hs from the phenyl (**Cat1**^{OTf}) or pyrazole (**Cat2**^{OTf}–**Cat4**^{OTf}) ring. Mean values of the $\Delta G_{binding}^{298}$ represented with intervals corresponding to one (green), two (yellow), and three (red) standard deviations.

In order to evaluate the participation of the silver(I) cation in the binding process, the titration with NaOTf was also performed for **Cat4**^{OTf} (K^{298} = 2.8±0.6; $\Delta G_{binding}^{298}$ = –2.6 kJ mol^{-1}). Taking into account that the binding energy for the titrations of by **Cat4**^{OTf} AgOTf and NaOTf does not overlap within 3 st. dev., silver(I) center participates to the binding process and thus changes of the chemical shift by binding of the catalyst σ-hole and excess TfO^- should be ruled out. Moreover, for the titration utilizing NaOTf, the chemical shift changed within narrower interval than that for AgOTf and this region was comparable to that for the titration of **Cat1**^{OTf} by AgOTf (**Figure 5**). This observation can indirectly indicate that for **Cat2**^{OTf}–**Cat4**^{OTf} species, the corresponding cations are ligated to the silver(I) center via the pyrazole N atom and the observed change in the chemical shift is not provided by simple binding of the triflate by the iodolium cation.

Combining the XRD and titration data, in the simplest case, the following binding modes including iodolium–silver(I) cooperation can be suggested (**Scheme 1**). Silver(I) center can ligate the iodolium cation via the pyrazole N atom (**Mode A**). The obtained dication can bind the triflate via the silver(I) center (**Mode B**) or one of the iodine(III)-centered σ-holes (**Mode C**). Due to complexity of the system, many other binding modes—involving more primary species, as it was realized for $[Ag_2(\mathbf{Cat4})_2(MeOH)_2(OTf)_2](OTf)_2$—also can be suggested, but their formation in the solution might be suppressed by the entropy factor. The binding **modes A**–**C** cannot be realized for **Cat1**$^+$ and thus additional mode should be suggested, which involves the I^{III}–Ag^I binding via the bridging triflate anion (**Mode D**).

Considering the low binding energy between the iodolium salts and AgOTf estimated from the titration experiments, the involvement of the solvent molecules to the consideration of the association process might have a significant impact on the total energy profile of the binding.[54, 68] Thus, the MeOH molecules were taken in explicit form for DFT calculations focused on estimation of relative energy of the key binding **modes A** and **D** (**Scheme 2**).

The obtained results indicate that the **mode A** is energetically favorable for **Cat2**$^+$–**Cat4**$^+$ species, although the estimated Gibbs free energy of binding is relatively low ($\Delta G_{binding}$ lay in the interval from –15.8 kJ mol^{-1} to –30.0 kJ mol^{-1}). These values can be explained in terms of electrostatic repulsion from the convergence of two cations. **Mode D** is significantly less energetically favorable. Even during consideration of the associated form of the silver(I) triflate as a referent point, this binding process is associated with change of $\Delta G_{binding}$ in the range from –6.8 kJ mol^{-1} to 2.6 kJ mol^{-1} (for the most energetically favorable binding). These results indicate that although **mode D** is imaginable for **Cat1**$^+$–**Cat4**$^+$ species in the solution, it likely does not make a significant contribution to the association processes. And vice versa, ligation of the iodolium cations to the silver(I) center via the pyrazole N atom (**Mode A** and correspondingly **modes B** and **C**) seems to provide significant impact into the binding of these species.

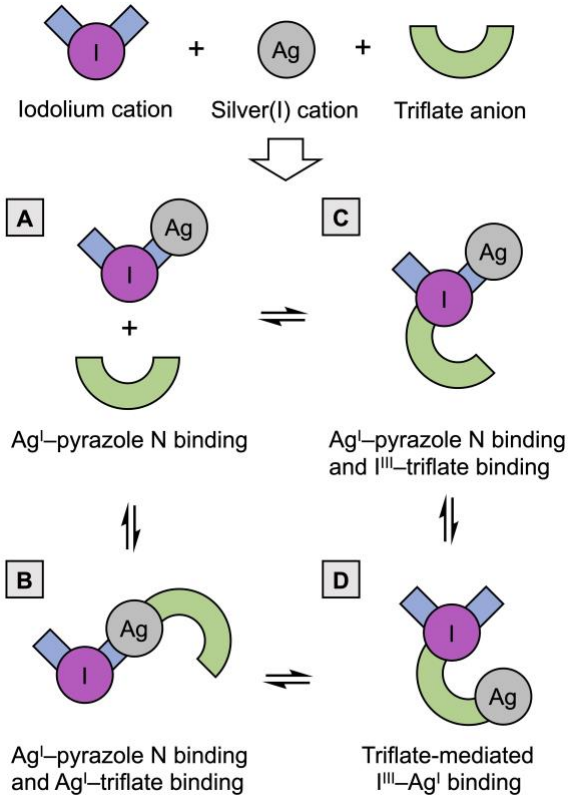

Scheme 1. Possible binding modes between the iodolium triflates and AgOTf in the solution.

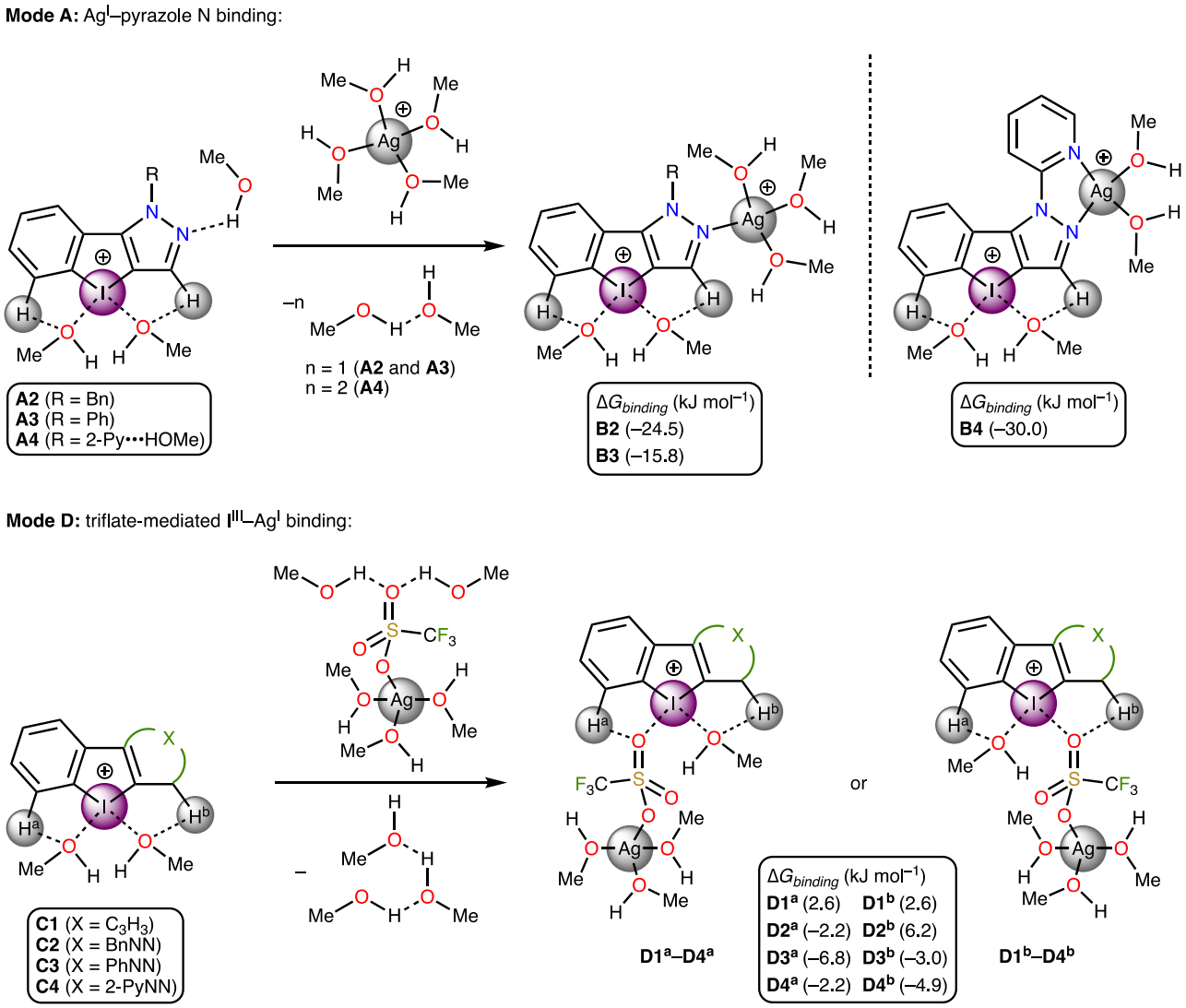

Scheme 2. Plausible key binding modes and the calculated corresponding values of the Gibbs free energy of the processes.

Cooperative electrophilic activation of organic species by the iodoliums and silver(I) center. For verification of the interplay between the iodine(III) and silver(I) centers during the electrophilic activation of organic species, three types of reactions have been chosen: (*i*) the reaction effectively catalyzed by both the iodine(III) and silver(I) centers, (*ii*) the reaction predominantly catalyzed by the iodine(III) center, and (*iii*) the reaction predominantly catalyzed by the silver(I) center.

(i) The iodine(III)- and silver(I)-catalyzed reaction. Many reactions requiring electrophilic activation of the substrates can be catalyzed by both XB-donors and metal-based Lewis acids. Considering that in our previous works we used as a model the multicomponent Groebke–Blackburn–Bienaymé reaction,[30, 54, 69] we used it in this work. The first step of this reaction—namely, reversible amine–aldehyde coupling giving a Schiff base (**Figure 6**, left)—was carried out in the presence of AgOTf (10 mol %), or any of **Cat1**^{OTf}–**Cat4**^{OTf} (10 mol %), or the mixture of any of **Cat1**^{OTf}–**Cat4**^{OTf} and AgOTf (1:1, total 20 mol % of the electrophiles). The kinetic data indicate that indeed this reaction is expectedly catalyzed either the silver(I) triflate and the iodolium triflates (**Table 2**, entries 1, 2, 3, 5, 7, 9). Rough approximation of the expected reaction rate constants for separate catalysis of the reaction by the mixture of silver(I) and iodine(III) centers [k_f(AgOTf+**Cat**^{OTf}) = k_f(AgOTf) + k_f(**Cat**^{OTf}) – k_f (non-catalyzed)] gives the following estimated values of the rate constants: k_f(AgOTf+**Cat1**^{OTf}) = 3.60 × 10^{-4} M^{-1} s^{-1}, k_f(AgOTf+**Cat2**^{OTf}) = 4.68 × 10^{-4} M^{-1} s^{-1}, k_f(AgOTf+**Cat3**^{OTf}) = 5.14 × 10^{-4} M^{-1} s^{-1}, k_f(AgOTf+**Cat1**^{OTf}) = 5.31 × 10^{-4} M^{-1} s^{-1}. Although this comparison has a qualitative character, the obtained experimental values of the rate constants for the reaction catalyzed by the mixture of **Cat**^{OTf} and AgOTf are significantly lower than that expected for the separate catalysis. Moreover, for the reaction catalyzed by **Cat2**^{OTf}, addition of AgOTf does not provide any acceleration of the reaction (entries 5 and 6). The higher relative acceleration of the reaction is observed for the mixture containing **Cat1**^{OTf}, which is not able to directly bind the silver(I) center via **modes A**–**C**. All these observations indicate that in the reaction solution strong interplay of the iodolium salts **Cat2**^{OTf}–**Cat4**^{OTf} and silver(I) center takes place. Suppression of the catalytic activity in the case of **Cat1**^{OTf} might be explained in terms of realization of **mode D** occupying one of the σ-holes at the iodine(III) center and one coordination site at the silver(I) center or competitive binding of the Lewis acids by excess triflate anions.

(ii) The iodine(III)-catalyzed reaction. The second step of the Groebke–Blackburn–Bienaymé reaction involving nucleophilic attack of the isocyanide on the imine C atom was used for the estimation of the catalytic effect of the iodolium salts in the presence of AgOTf (**Figure 6**, right). The silver(I) center does not

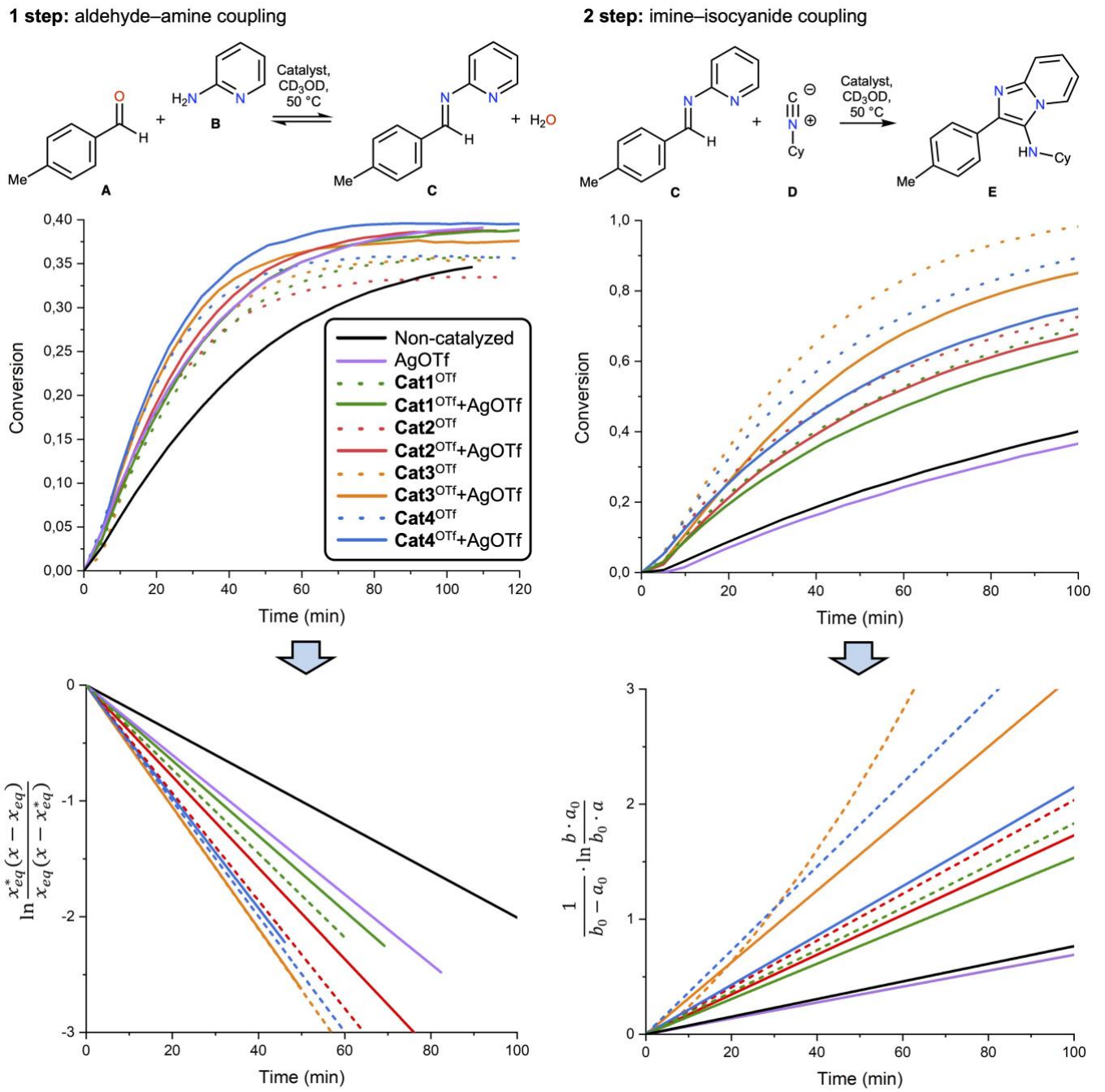

Figure 6. The Groebke–Blackburn–Bienaymé reaction carried out stepwisely in the presence of the electrophilic activators and the corresponding kinetic plots based on the ^{1}H NMR monitoring.

provide the catalytic effect on the isocyanide–imine coupling and moreover it slightly inhibits the reaction (**Table 2**, entries 1 and 2). The kinetic data unambiguously indicate that the catalytic activity of **Cat1**^{OTf}–**Cat4**^{OTf} (10 mol %) is reduced by the AgOTf (10 mol %; entries 3–10). The most significant reduction of the catalytic effect is observed for **Cat4**^{OTf}, whose binding energy with the silver(I) center were computationally estimated to be the highest among **Cat1**^{OTf}–**Cat4**^{OTf}. Noteworthy that although the silver(I) triflate reduces the catalytic activity of the iodolium salts, it prevents their decomposition in the progress of the reaction, which was observed for **Cat3**^{OTf} and **Cat4**^{OTf} by us in this work and previously.[54]

(iii) The silver(I)-catalyzed reaction. The intramolecular nucleophilic attack on the alkyne C≡C bond in the reaction chosen as a model does not proceed in the absence of the silver(I) center (**Scheme 3**). It was found that carbamate **F** totally transforms into **H**

Table 2. The rate constants for first and second steps of the Groebke–Blackburn–Bienaymé reaction calculated from the experimental kinetic data.

Entry	Catalytic system	First step	Second step
		$k_f \times 10^4$ (M^{-1} s^{-1})	$k \times 10^4$ (M^{-1} s^{-1})
1	Non-catalyzed	1.81(1)	1.28(2)
2	AgOTf	2.90(2)	1.15(6)
3	**Cat1**^{OTf}	2.51(2)	3.06(1)
4	**Cat1**^{OTf}+AgOTf	3.08(3)	2.56(2)
5	**Cat2**^{OTf}	3.59(7)	3.39(3)
6	**Cat2**^{OTf}+AgOTf	3.62(3)	2.88(2)
7	**Cat3**^{OTf}	4.05(5)	9.8(4)
8	**Cat3**^{OTf}+AgOTf	4.45(8)	5.21(3)
9	**Cat4**^{OTf}	4.22(4)	6.07(4)
10	**Cat4**^{OTf}+AgOTf	4.43(1)	3.58(1)

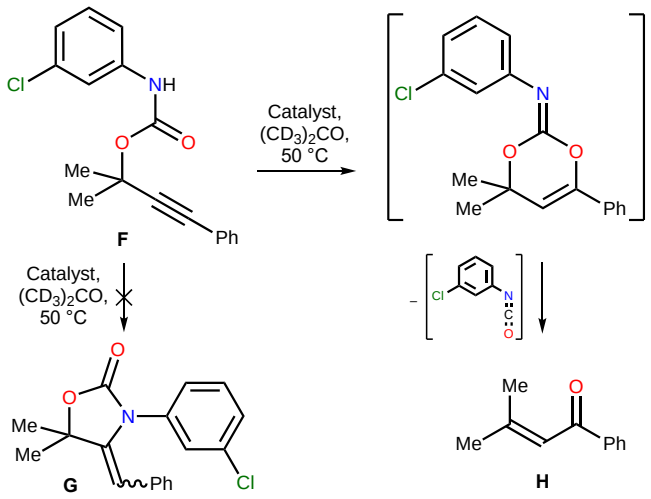

Catalyst	Yield **H** (3.5 h)	Yield **H** (25 h)
–	0%	0%
Cat4^{OTf}	0%	0%
AgOTf	53%	100%
AgOTf+**Cat4**^{OTf}	17%	95%

Scheme 3. Silver(I)-catalyzed intramolecular nucleophilic attack of the O atom on the alkyne and the plausible intermediate of reaction. ^{1}H NMR yield of **H** is represented in the box.

in the presence of AgOTf (20 mol %) within 25 h at 50 °C in Me_2CO (MeOH was inapplicable for the monitoring due to heterogeneity of the mixture), whereas addition of **Cat4**^{OTf} (20 mol %) reduces its catalytic activity. Thus, after 3.5 h from the beginning of the reaction, AgOTf led to the formation of **H** with 53% yield based on ^{1}H NMR, whereas addition of **Cat4**^{OTf} to this system results in the 17% yield of **H** after the same period. 3-Chlorophenyl isocyanate was detected in the reaction mixture along with a small amount of the cyanate-derived side-products (3-chloroaniline and *N*,*N*'-di(3-chlorophenyl)urea were identified by HRESI$^+$-MS). Noticeably that the expected[70] heterocyclic compound **G** was not detected in the reaction mixture, which can be explained by the absence of a base in the reaction mixture.

Conclusions

Results of this work are at least three-fold. Firstly, it was shown on the model iodolium–silver(I) system that XB-donating species can interact with metal-based Lewis acids during the electrophilic activation of organic species. Their interplay might represent a complex set of reversible binding processes, which affect the total catalytic activity of the system. Although no synergetic effect has been found in the studied system and some suppression of the total catalytic activity was found during the XB-donor–metal cation cooperation in this work, we hope that our study will play a role of a foothold for further development of efficient bifunctional hybrid organic–inorganic catalysts based on utilization of XB-donors, as well as other σ-hole donors covering chalcogen- or pnictogen-bonding species.

Secondly, in this work, unprecedent example of higher catalytic activity of XB-donating species compared to the conventional Lewis acid has been shown. Although the XB-donating species are considered as an ecological alternative to traditional heavy metal-based Lewis acids, many previous works indicated that the catalytic activity based on electrophilic activation of organic substrates of such organocatalysts is incomparably lower than that of traditional metal-complex catalysts. Thus, it was found that the potential of utilization of σ-hole donors in organocatalysis is higher than it was considered previously, since they effectively catalyze reactions, which are not accelerated by some metal-containing Lewis acids.

Thirdly, it was found that silver(I) triflate stabilize the pyrazole-containing iodolium cations during the reaction progress and thus complexation of XB-donors with the metal center can prevent their decomposition as it was found for other examples of organic substrates,[71, 72] but has not been shown for XB-donating organocatalytic species. This observation may allow one to obtain new types of organocatalytic species ligated to a metal center, which are not stable in the free state.

Experimental Section

Materials and instrumentation. All solvents, aldehydes, isocyanides, 2-aminopyridine, AgOTf and NaOTf were obtained from commercial sources and used as received. The iodonium salts **Cat1**^{OTf}–**Cat4**^{OTf} were synthesized according to published procedures.[29, 31] All syntheses were conducted in air. Chromatographic separation was carried out using Macherey-Nagel silica gel 60 M (0.063–0.2 mm). Analytical TLC was performed on unmodified Merck ready-to-use plates (TLC silica gel 60 F254) with UV detection. Melting points were measured on a Stuart SMP30 apparatus in capillaries and are not corrected. Electrospray ionization mass-spectra were obtained on a Bruker maXis spectrometer equipped with an electrospray ionization (ESI) source. The instrument was operated in positive ion mode using an *m*/*z* range 50–1200. The nebulizer gas flow was 1.0 bar and the drying gas flow 4.0 L min^{-1}. For HRESI$^+$, the studied compounds were dissolved in MeOH. ^{1}H- and ^{13}C{^{1}H} NMR spectra were measured on a Bruker Avance 400 spectrometer in $CDCl_3$, CD_3OD and $(CD_3)_2SO$ at 298 K; the residual solvent signal was used as the internal standard. The NMR monitoring kinetic experiments were carried out by measuring the ^{1}H NMR spectra every 5 min (four scans; repetition time = 4 s) following the initial equilibration period of 5 min on a Bruker Avance III 500 spectrometer in CD_3OD at 50 °C; the residual solvent signal was used as the internal standard.

Single-crystal XRD study. Single-crystal X-ray diffraction experiments were carried out on Agilent Technologies «Xcalibur» and «SuperNova» diffractometers with monochromated MoKα or CuKα radiation, respectively. Crystals were kept at 100(2) K during data collection. Structures have been solved by the Superflip,[73, 74] and the ShelXT[75] structure solution programs using Charge Flipping and Intrinsic Phasing and refined by means of the ShelXL program[76] incorporated in the OLEX2 program package.[77] The crystal data and details of structure refinements for **Cat1**$_3$[Ag(OTf)$_4$] and [Ag$_2$(**Cat4**)$_2$(MeOH)$_2$(OTf)$_2$](OTf)$_2$ are shown in **Table S1**.

^{1}H NMR titration. A portion of AgOTf (from 1- to 20-fold excess) was added to a series of solutions of **Cat1**^{OTf}–**Cat4**^{OTf} and a portion of NaOTf (from 1- to 20-fold excess) was added to **Cat4**^{OTf} in CD_3OD (17.75 mM, 600 μL). The ^{1}H NMR spectra were measured at 298 K. K^{298} values are calculated using Bindfit software using a 1:1 host–guest binding model.

^{1}H NMR Monitoring of the first step of the reaction. The 4-tolylaldehyde (51.8 μL, 0.439 mmol), 2-aminopyridine (10.3 mg, 0.110 mmol) and AgOTf (2.8 mg, 0.011 mmol) were added to the CD_3OD solution of **Cat1**^{OTf}–**Cat4**^{OTf} (18.3 mM, 600 μL, 0.011 mmol) and placed in an NMR tube. For the noncatalyzed reaction, the same quantities of the reactants were added to CD_3OD (600 μL) and

placed in an NMR tube. The NMR tube was then sealed, and the obtained homogeneous solution was maintained at 50 °C for 100 min in the NMR spectrometer. The reaction was monitored by measuring the time-dependent integral density of the 4-tolylaldehyde and imine proton group signals.

^{1}H NMR monitoring of the second step of the reaction. The imine (86 mg, 0.439 mmol), cyclohexyl isocyanide (13.6 μL, 0.110 mmol) and AgOTf (2.8 mg, 0.011 mmol) were added to the CD_3OD solution of **Cat1**^{OTf}–**Cat4**^{OTf} (18.3 mM, 600 μL, 0.011 mmol) and placed in an NMR tube. For the noncatalyzed reaction, the same quantities of the reactants were added to the CD_3OD (600 μL) and placed in an NMR tube. The NMR tube was sealed, and the obtained homogeneous solution was maintained at 50 °C for 100 min in an NMR spectrometer. The reaction was monitored by measuring the time-dependent integral density of the ipso-cyclohexyl proton group signals in isocyanide and in the product of the reaction.

Computational details. The single point calculations based on the experimental X-ray geometry of **Cat1**$_3$[Ag(OTf)$_4$] and geometry optimization procedure for square-planar and tetrahedral isomers of [Ag(OTf)$_4$]$^{3-}$ have been carried out at the DFT level of theory using the dispersion-corrected hybrid functional ωB97XD[78] with the help of Gaussian-09[79] program package. The Sapporo-DZP basis sets[80] were used for all atoms. The topological analysis of the electron density distribution with the help of the atoms in molecules (QTAIM) method, electron localization function (ELF), reduced density gradient (RDG), and non-covalent interactions (NCI) analyses have been performed by using the Multiwfn program (version 3.7).[81] The Cartesian atomic coordinates for appropriate model structures are presented in **Table S2**, Supporting Information.

The full geometry optimization of all model structures in methanol solution was carried out at the DFT level of theory using the M06-2X functional[82] with the help of the Gaussian-09 program package.[79] The quasi-relativistic MWB28 and MWB46 pseudopotentials,[83] which described 28 and 46 core electrons, and the appropriate contracted basis sets were used for silver and iodine atoms, respectively, while the standard 6-31G* basis sets were used for other atoms. No symmetry restrictions were applied during the geometry optimizations. The solvent effects were taken into account using the SMD (Solvation Model based on Density) continuum solvation model suggested by Truhlar and coworkers.[84] The Hessian matrices were calculated analytically for all optimized model structures to prove the location of the correct minimum on the potential energy surface (no imaginary frequencies). The Cartesian atomic coordinates for all appropriate model structures are presented in xyz-file (Supporting Information).

Conflicts of interest

There are no conflicts to declare.

Acknowledgements

This multidisciplinary study was supported by the Russian Science Foundation (grant 23-23-00091, physicochemical study and preparation of the complexes), Saint Petersburg State University (grant 101746143; synthesis of the organic substrates), and RUDN University Strategic Academic Leadership Program (DFT calculations). Physicochemical studies were performed at the Center for Magnetic Resonance, Center for X-ray Diffraction Studies, and Center for Chemical Analysis and Materials Research (all at Saint Petersburg State University).

Electronic supplementary information: S

^{1}H NMR monitoring of the Groebke–Blackburn–Bienaymé reaction; ^{1}H NMR Monitoring of the first step of the reaction; ^{1}H NMR monitoring of the second step of the reaction; ^{1}H NMR monitoring of the silver(I)-catalyzed intermolecular rearrangement; ^{1}H NMR titration data; Synthesis and characterization of **C**, **F** and **H**; Synthesis and characterization of **Cat1**^{OTf}–**Cat4**^{OTf}; Spectra of **C**, **F**, **H**, **Cat1**^{OTf}–**Cat4**^{OTf}; **Table S1.** Crystal data for **Cat1**$_3$[Ag(OTf)$_4$] and [Ag$_2$(**Cat4**)$_2$(MeOH)$_2$(OTf)$_2$](OTf)$_2$; Details of QTAIM analysis; **Table S2**. Cartesian atomic coordinates for model structures; **Table S3**. Calculated total electronic energies, enthalpies, Gibbs free energies, and entropies for optimized equilibrium model structures.

References

1. V. Oliveira, M. Cardoso and L. Forezi, Organocatalysis: A Brief Overview on Its Evolution and Applications, *Catalysts*, 2018, **8**, 605.
2. Y. Qin, L. Zhu and S. Luo, Organocatalysis in Inert C-H Bond Functionalization, *Chem. Rev.*, 2017, **117**, 9433–9520.
3. T. Chanda and J. C. G. Zhao, Recent Progress in Organocatalytic Asymmetric Domino Transformations, *Adv. Synth. Catal.*, 2018, **360**, 2–79.
4. S. Vellalath and D. Romo, Asymmetric Organocatalysis: The Emerging Utility of alpha,beta-Unsaturated Acylammonium Salts, *Angew. Chem. Int. Ed.*, 2016, **55**, 13934–13943.
5. Z. Begum, C. Seki, Y. Okuyama, E. Kwon, K. Uwai, M. Tokiwa, S. Tokiwa, M. Takeshita and H. Nakano, New boro amino amide organocatalysts for asymmetric cross aldol reaction of ketones with carbonyl compounds, *RSC Adv.*, 2023, **13**, 888–894.
6. H. Guo, Y. C. Fan, Z. Sun, Y. Wu and O. Kwon, Phosphine Organocatalysis, *Chem. Rev.*, 2018, **118**, 10049–10293.
7. D. M. Flanigan, F. Romanov-Michailidis, N. A. White and T. Rovis, Organocatalytic Reactions Enabled by N-Heterocyclic Carbenes, *Chem. Rev.*, 2015, **115**, 9307–9387.
8. S. Mondal, S. R. Yetra, S. Mukherjee and A. T. Biju, NHC-Catalyzed Generation of alpha,beta-Unsaturated Acylazoliums for the Enantioselective Synthesis of Heterocycles and Carbocycles, *Acc. Chem. Res.*, 2019, **52**, 425–436.
9. M. N. Grayson and K. N. Houk, Cinchona Urea-Catalyzed Asymmetric Sulfa-Michael Reactions: The Bronsted Acid-Hydrogen Bonding Model, *J. Am. Chem. Soc.*, 2016, **138**, 9041–9044.
10. M. Puripat, R. Ramozzi, M. Hatanaka, W. Parasuk, V. Parasuk and K. Morokuma, The Biginelli Reaction Is a Urea-Catalyzed Organocatalytic Multicomponent Reaction, *J. Org. Chem.*, 2015, **80**, 6959–6967.
11. N. Busschaert, C. Caltagirone, W. Van Rossom and P. A. Gale, Applications of Supramolecular Anion Recognition, *Chem. Rev.*, 2015, **115**, 8038–8155.
12. X. Fang and C. J. Wang, Recent advances in asymmetric organocatalysis mediated by bifunctional amine-thioureas bearing multiple hydrogen-bonding donors, *Chem. Commun.*, 2015, **51**, 1185–1197.
13. O. V. Serdyuk, C. M. Heckel and S. B. Tsogoeva, Bifunctional primary amine-thioureas in asymmetric organocatalysis, *Org. Biomol. Chem.*, 2013, **11**, 7051–7071.
14. F. E. Held and S. B. Tsogoeva, Asymmetric cycloaddition reactions catalyzed by bifunctional thiourea and squaramide organocatalysts: recent advances, *Catal. Sci. Technol.*, 2016, **6**, 645–667.

15. X. Han, H. B. Zhou and C. Dong, Applications of Chiral Squaramides: From Asymmetric Organocatalysis to Biologically Active Compounds, *Chem. Rec.*, 2016, **16**, 897–906.
16. B. L. Zhao, J. H. Li and D. M. Du, Squaramide-Catalyzed Asymmetric Reactions, *Chem. Rec.*, 2017, **17**, 994–1018.
17. D. Parmar, E. Sugiono, S. Raja and M. Rueping, Complete field guide to asymmetric BINOL-phosphate derived Bronsted acid and metal catalysis: history and classification by mode of activation; Bronsted acidity, hydrogen bonding, ion pairing, and metal phosphates, *Chem. Rev.*, 2014, **114**, 9047–9153.
18. T. Akiyama and K. Mori, Stronger Bronsted Acids: Recent Progress, *Chem. Rev.*, 2015, **115**, 9277-9306.
19. T. James, M. van Gemmeren and B. List, Development and Applications of Disulfonimides in Enantioselective Organocatalysis, *Chem. Rev.*, 2015, **115**, 9388–9409.
20. G. Cavallo, P. Metrangolo, R. Milani, T. Pilati, A. Priimagi, G. Resnati and G. Terraneo, The Halogen Bond, *Chem. Rev.*, 2016, **116**, 2478–2601.
21. L. Vogel, P. Wonner and S. M. Huber, Chalcogen Bonding: An Overview, *Angew. Chem. Int. Ed.*, 2019, **58**, 1880-1891.
22. S. Portela, J. J. Cabrera-Trujillo and I. Fernandez, Catalysis by Bidentate Iodine(III)-Based Halogen Donors: Surpassing the Activity of Strong Lewis Acids, *J. Org. Chem.*, 2021, **86**, 5317–5326.
23. R. Robidas, D. L. Reinhard, C. Y. Legault and S. M. Huber, Iodine(III)-Based Halogen Bond Donors: Properties and Applications, *Chem. Rec.*, 2021, **21**, 1912–1927.
24. F. Heinen, E. Engelage, C. J. Cramer and S. M. Huber, Hypervalent Iodine(III) Compounds as Biaxial Halogen Bond Donors, *J. Am. Chem. Soc.*, 2020, **142**, 8633–8640.
25. A. Boelke, T. J. Kuczmera, E. Lork and B. J. Nachtsheim, N-Heterocyclic Iod(az)olium Salts - Potent Halogen-Bond Donors in Organocatalysis, *Chem.–Eur. J.*, 2021, **27**, 13128–13134.
26. F. Heinen, D. L. Reinhard, E. Engelage and S. M. Huber, A Bidentate Iodine(III)-Based Halogen-Bond Donor as a Powerful Organocatalyst, *Angew. Chem. Int. Ed.*, 2021, **60**, 5069–5073.
27. Y. Nishida, T. Suzuki, Y. Takagi, E. Amma, R. Tajima, S. Kuwano and T. Arai, A Hypervalent Cyclic Dibenzoiodolium Salt as a Halogen-Bond-Donor Catalyst for the [4+2] Cycloaddition of 2-Alkenylindoles, *ChemPlusChem*, 2021, **86**, 741–744.
28. R. Haraguchi, T. Nishikawa, A. Kanazawa and S. Aoshima, Metal-Free Living Cationic Polymerization Using Diaryliodonium Salts as Organic Lewis Acid Catalysts, *Macromolecules*, 2020, **53**, 4185–4192.
29. S. N. Yunusova, A. S. Novikov, N. S. Soldatova, M. A. Vovk and D. S. Bolotin, Iodonium salts as efficient iodine(iii)-based noncovalent organocatalysts for Knorr-type reactions, *RSC Adv.*, 2021, **11**, 4574–4583.
30. M. V. Il'in, A. A. Sysoeva, A. S. Novikov and D. S. Bolotin, Diaryliodoniums as Hybrid Hydrogen- and Halogen-Bond-Donating Organocatalysts for the Groebke-Blackburn-Bienayme Reaction, *J. Org. Chem.*, 2022, **87**, 4569–4579.
31. A. Boelke, T. J. Kuczmera, L. D. Caspers, E. Lork and B. J. Nachtsheim, Iodolopyrazolium Salts: Synthesis, Derivatizations, and Applications, *Org. Lett.*, 2020, **22**, 7261–7266.
32. X. Peng, A. Rahim, W. Peng, F. Jiang, Z. Gu and S. Wen, Recent Progress in Cyclic Aryliodonium Chemistry: Syntheses and Applications, *Chem. Rev.*, 2023, DOI: 10.1021/acs.chemrev.2c00591.
33. D. S. Bolotin, N. A. Bokach, M. Y. Demakova and V. Y. Kukushkin, Metal-Involving Synthesis and Reactions of Oximes, *Chem. Rev.*, 2017, **117**, 13039–13122.
34. H. M. L. Davies and D. Morton, Recent Advances in C-H Functionalization, *J. Org. Chem.*, 2016, **81**, 343–350.
35. A. Dey, S. Agasti and D. Maiti, Palladium Catalysed meta-C-H Functionalization Reactions, *Org. Biomol. Chem.*, 2016, **14**, 5440–5453.
36. Z. Fan, J. Li, H. Lu, D. Y. Wang, C. Wang, M. Uchiyama and A. Zhang, Monomeric Octahedral Ruthenium(II) Complex Enabled meta-C-H Nitration of Arenes with Removable Auxiliaries, *Org. Lett.*, 2017, **19**, 3199–3202.
37. Z. Fan, J. Ni and A. Zhang, Meta-Selective CAr-H Nitration of Arenes through a $Ru_3(CO)_{12}$-Catalyzed Ortho-Metalation Strategy, *J. Am. Chem. Soc.*, 2016, **138**, 8470–8475.
38. C. G. Frost and A. J. Paterson, Directing Remote Meta-C-H Functionalization with Cleavable Auxiliaries, *ACS Cent. Sci.*, 2015, **1**, 418–419.
39. L. Liu, Q. Wang, R. Zhu and J. Huang, A Massé Shot: Transition-Metal-Catalyzed Selective *meta*-C–H Functionalization (ortho-Metallation and para-Bromination Relay), *Synlett*, 2016, **27**, 1450–1455.
40. D. A. Petrone, J. Ye and M. Lautens, Modern Transition-Metal-Catalyzed Carbon-Halogen Bond Formation, *Chem. Rev.*, 2016, **116**, 8003–8104.
41. J. Yang, Transition Metal Catalyzed *meta*-C–H Functionalization of Aromatic Compounds, *Org. Biomol. Chem.*, 2015, **13**, 1930–1941.
42. D. Wang and D. Astruc, The golden age of transfer hydrogenation, *Chem. Rev.*, 2015, **115**, 6621–6686.
43. Q. A. Chen, Z. S. Ye, Y. Duan and Y. G. Zhou, Homogeneous palladium-catalyzed asymmetric hydrogenation, *Chem. Soc. Rev.*, 2013, **42**, 497–511.
44. Y. Nakajima and S. Shimada, Hydrosilylation reaction of olefins: recent advances and perspectives, *RSC Adv.*, 2015, **5**, 20603–20616.
45. J. Y. Corey, Reactions of Hydrosilanes with Transition Metal Complexes, *Chem. Rev.*, 2016, **116**, 11291–11435.
46. G. Jindal, H. K. Kisan and R. B. Sunoj, Mechanistic Insights on Cooperative Catalysis through Computational Quantum Chemical Methods, *ACS Catal.*, 2014, **5**, 480–503.
47. S. P. Sancheti, Urvashi, M. P. Shah and N. T. Patil, Ternary Catalysis: A Stepping Stone toward Multicatalysis, *ACS Catal.*, 2020, **10**, 3462–3489.
48. S. Afewerki and A. Cordova, Combinations of Aminocatalysts and Metal Catalysts: A Powerful Cooperative Approach in Selective Organic Synthesis, *Chem. Rev.*, 2016, **116**, 13512–13570.
49. K. Guillier, E. Caytan, V. Dorcet, F. Mongin, E. Dumont and F. Chevallier, A Halogen-Bond Donor Catalyst for Templated Macrocyclization, *Angew. Chem. Int. Ed.*, 2019, **58**, 14940–14943.
50. J. Wolf, F. Huber, N. Erochok, F. Heinen, V. Guerin, C. Y. Legault, S. F. Kirsch and S. M. Huber, Activation of a Metal-Halogen Bond by Halogen Bonding, *Angew. Chem. Int. Ed.*, 2020, **59**, 16496–16500.
51. H. F. Jónsson, D. Sethio, J. Wolf, S. M. Huber, A. Fiksdahl and M. Erdelyi, Halogen Bond Activation in Gold Catalysis, *ACS Catal.*, 2022, **12**, 7210–7220.
52. F. Heinen, E. Engelage, A. Dreger, R. Weiss and S. M. Huber, Iodine(III) Derivatives as Halogen Bonding Organocatalysts, *Angew. Chem. Int. Ed.*, 2018, **57**, 3830–3833.
53. D. L. Reinhard, F. Heinen, J. Stoesser, E. Engelage and S. M. Huber, Tuning the Halogen Bonding Strength of Cyclic Diaryliodonium Salts, *Helv. Chim. Acta*, 2021, **104**, e2000221.
54. D. A. Polonnikov, M. V. Il'in, Y. V. Safinskaya, I. S. Aliyarova, A. S. Novikov and D. S. Bolotin, (Pre)association as a crucial step for

computational prediction and analysis of the catalytic activity of σ-hole donating organocatalysts, *Org. Chem. Front.*, 2023, **10**, 169–180.
55. M. Z. Lu, J. Goh, M. Maraswami, Z. Jia, J. S. Tian and T. P. Loh, Recent Advances in Alkenyl sp(2) C-H and C-F Bond Functionalizations: Scope, Mechanism, and Applications, *Chem. Rev.*, 2022, **122**, 17479–17646.
56. I. P. Beletskaya and V. P. Ananikov, Transition-Metal-Catalyzed C-S, C-Se, and C-Te Bond Formations via Cross-Coupling and Atom-Economic Addition Reactions. Achievements and Challenges, *Chem. Rev.*, 2022, **122**, 16110–16293.
57. M. Alvarez-Corral, M. Munoz-Dorado and I. Rodriguez-Garcia, Silver-Mediated Synthesis of Heterocycles, *Chem. Rev.*, 2008, **108**, 3174–3198.
58. G. Fang and X. Bi, Silver-catalysed reactions of alkynes: recent advances, *Chem. Soc. Rev.*, 2015, **44**, 8124–8173.
59. A. G. Young and L. R. Hanton, Square planar silver(I) complexes: A rare but increasingly observed stereochemistry for silver(I), *Coord. Chem. Rev.*, 2008, **252**, 1346–1386.
60. R. F. W. Bader, A quantum theory of molecular structure and its applications, *Chem. Rev.*, 1991, **91**, 893–928.
61. A. Bondi, Van der Waals volumes and radii of metals in covalent compounds, *J. Phys. Chem.*, 1966, **70**, 3006–3007.
62. E. V. Bartashevich and V. G. Tsirelson, Interplay between non-covalent interactions in complexes and crystals with halogen bonds, *Russ. Chem. Rev.*, 2014, **83**, 1181–1203.
63. E. Espinosa, I. Alkorta, J. Elguero and E. Molins, From weak to strong interactions: A comprehensive analysis of the topological and energetic properties of the electron density distribution involving X–H···F–Y systems, *J. Chem. Phys.*, 2002, **117**, 5529–5542.
64. E. R. Johnson, S. Keinan, P. Mori-Sanchez, J. Contreras-Garcia, A. J. Cohen and W. Yang, Revealing Noncovalent Interactions, *J. Am. Chem. Soc.*, 2010, **132**, 6498–6506.
65. J. Contreras-García, E. R. Johnson, S. Keinan, R. Chaudret, J.-P. Piquemal, D. N. Beratan and W. Yang, NCIPLOT: a program for plotting non-covalent interaction regions, *J. Chem. Theory Comput.*, 2011, **7**, 625–632.
66. D. S. Bolotin, N. S. Soldatova, M. Y. Demakova, A. S. Novikov, D. M. Ivanov, I. S. Aliyarova, A. Sapegin and M. Krasavin, Pentacoordinated silver(I) complex featuring 8-phenylquinoline ligands: Interplay of coordination bonds, semicoordination, and stacking interactions, *Inorg. Chim. Acta*, 2020, **504**, 119453.
67. J. Burgess and P. J. Steel, Is the silver–alkene interaction a useful new supramolecular synthon?, *Coord. Chem. Rev.*, 2011, **255**, 2094-2103.
68. L. L. Han, S. J. Li and D. C. Fang, Theoretical estimation of kinetic parameters for nucleophilic substitution reactions in solution: an application of a solution translational entropy model, *Phys. Chem. Chem. Phys.,* 2016, **18**, 6182–6190.
69. M. V. Il'in, A. S. Novikov and D. S. Bolotin, Sulfonium and Selenonium Salts as Noncovalent Organocatalysts for the Multicomponent Groebke-Blackburn-Bienayme Reaction, *J Org Chem*, 2022, **87**, 10199–10207.
70. T. Yamada, K. Sekine and T. Mawatari, Synthesis of Oxazolidin-2-ones by Tandem Cyclization of Propargylic Alcohols and Phenyl Isocyanate Promoted by Silver Catalysts as π-Lewis Acids, *Synlett*, 2015, **26**, 2447–2450.
71. D. S. Bolotin, K. I. Kulish, N. A. Bokach, G. L. Starova, V. V. Gurzhiy and V. Y. Kukushkin, Zinc(II)-Mediated Nitrile–Amidoxime Coupling Gives New Insights into H(+)-Assisted Generation of 1,2,4-Oxadiazoles, *Inorg. Chem.*, 2014, **53**, 10312–10324.
72. D. S. Bolotin, N. A. Bokach, M. Haukka and V. Y. Kukushkin, Platinum(IV)-Mediated Nitrile-Amidoxime Coupling Reactions: Insights into the Mechanism for the Generation of 1,2,4-Oxadiazoles, *ChemPlusChem*, 2012, **77**, 31–40.
73. L. Palatinus and G. Chapuis, SUPERFLIP. A computer program for the solution of crystal structures by charge flipping in arbitrary dimensions, *J. Appl. Crystallogr.*, 2007, **40**, 786–790.
74. L. Palatinus, S. J. Prathapa and S. van Smaalen, EDMA: a computer program for topological analysis of discrete electron densities, *J. Appl. Crystallogr.*, 2012, **45**, 575–580.
75. G. M. Sheldrick, SHELXT - integrated space-group and crystal-structure determination, *Acta Crystallogr.*, 2015, **A71**, 3–8.
76. G. M. Sheldrick, Crystal structure refinement with SHELXL, *Acta Crystallogr.*, 2015, **C71**, 3–8.
77. O. V. Dolomanov, L. J. Bourhis, R. J. Gildea, J. A. K. Howard and H. Puschmann, OLEX2: A complete structure solution, refinement and analysis programm, *J. Appl. Crystallogr.*, 2009, **42**, 339–341.
78. J. D. Chai and M. Head-Gordon, Long-range corrected hybrid density functionals with damped atom-atom dispersion corrections, *Phys. Chem. Chem. Phys.,* 2008, **10**, 6615–6620.
79. M. J. Frisch, G. W. Trucks, H. B. Schlegel, G. E. Scuseria, M. A. Robb, J. R. Cheeseman, G. Scalmani, V. Barone, B. Mennucci, G. A. Petersson, H. Nakatsuji, M. Caricato, X. Li, H. P. Hratchian, A. F. Izmaylov, J. Bloino, G. Zheng, J. L. Sonnenberg, M. Hada, M. Ehara, K. Toyota, R. Fukuda, J. Hasegawa, M. Ishida, T. Nakajima, Y. Honda, O. Kitao, H. Nakai, T. Vreven, J. J. A. Montgomery, J. E. Peralta, F. Ogliaro, M. Bearpark, J. J. Heyd, E. Brothers, K. N. Kudin, V. N. Staroverov, T. Keith, R. Kobayashi, J. Normand, K. Raghavachari, A. Rendell, J. C. Burant, S. S. Iyengar, J. Tomasi, M. Cossi, N. Rega, J. M. Millam, M. Klene, J. E. Knox, J. B. Cross, V. Bakken, C. Adamo, J. Jaramillo, R. Gomperts, R. E. Stratmann, O. Yazyev, A. J. Austin, R. Cammi, C. Pomelli, J. W. Ochterski, R. L. Martin, K. Morokuma, V. G. Zakrzewski, G. A. Voth, P. Salvador, J. J. Dannenberg, S. Dapprich, A. D. Daniels, O. Farkas, J. B. Foresman, J. V. Ortiz, J. Cioslowski and D. J. Fox, Gaussian 09, Revision C.01., 2010.
80. B. P. Pritchard, D. Altarawy, B. Didier, T. D. Gibson and T. L. Windus, New Basis Set Exchange: An Open, Up-to-Date Resource for the Molecular Sciences Community, *J. Chem. Inf. Model*, 2019, **59**, 4814–4820.
81. T. Lu and F. Chen, Multiwfn: a multifunctional wavefunction analyzer, *J. Comput. Chem.*, 2012, **33**, 580–592.
82. Y. Zhao and D. G. Truhlar, The M06 suite of density functionals for main group thermochemistry, thermochemical kinetics, noncovalent interactions, excited states, and transition elements: two new functionals and systematic testing of four M06-class functionals and 12 other functionals, *Theor. Chem. Acc.*, 2007, **120**, 215–241.
83. A. Bergner, M. Dolg, W. Küchle, H. Stoll and H. Preuß, Ab initio energy-adjusted pseudopotentials for elements of groups 13–17, *Mol. Phys.*, 1993, **80**, 1431–1441.
84. A. V. Marenich, C. J. Cramer and D. G. Truhlar, Universal Solvation Model Based on Solute Electron Density and on a Continuum Model of the Solvent Defined by the Bulk Dielectric Constant and Atomic Surface Tensions, *J. Phys. Chem. B*, 2009, **113**, 6378–6396.